Charge and spin current pumping by ultrafast demagnetization dynamics

Jalil Varela-Manjarres, Ali Kefayati, M. Benjamin Jungfleisch, John Q. Xiao, and Branislav K. Nikolić*
Department of Physics and Astronomy, University of Delaware, Newark, DE 19716, USA

The surprising discovery of ultrafast *demagnetization*—where electric field of femtosecond laser pulse couples to electrons of a ferromagnetic (FM) layer causing its magnetization vector *to shrink while not rotating*, $M_z(t)/M_z(t=0) < 1$—is also assumed to be accompanied by generation of spin current in the direction orthogonal to electric field. However, understanding of the microscopic origin of such spin current, its frequency spectrum and how efficiently it can be converted into charge current, as the putative source of THz radiation, is lacking despite nearly three decades of intense studies. Conversely, quantum transport theory rigorously explains [Y. Tserkovnyak *et al.*, Rev. Mod. Phys. **77**, 1375 (2005)] how microwave driven precession of magnetization vector of *fixed* length $\mathbf{M}(t)$ leads to pumping of spin current $\propto \mathbf{M} \times d\mathbf{M}/dt$ into adjacent normal metal (NM) layers sandwiching FM layer to form two-terminal geometry without any applied bias voltage. Here we connect these two apparently disparate phenomena by *replacing* periodic time-dependence of magnetization precession with nonperiodic time-dependence of demagnetization, as obtained from experiments on ultrafast-light-driven Ni layer, within the same two-terminal setup of standard spin pumping theory. Applying time-dependent nonequilibrium Green's functions, able to evolve such setup with arbitrary time dependence, reveals how demagnetization dynamics pumps *both* charge and spin currents in directions both parallel and orthogonal to electric field of laser pulse, even in the absence of spin-orbit coupling and thereby induced spin-to-charge conversion mechanisms. Although pumped currents follow dM_z/dt in some setups, this becomes obscured when NM layers are disconnected and pumped currents start to reflect from FM boundaries (as is the case of experimental setups). Finally, we use the Jefimenko equations to compute electromagnetic radiation by charge current pumped in disconnected setup during demagnetization, or later during its slow recovery, unraveling that radiated electric field *only* in the former time interval exhibits features in 0.1–30 THz frequency range probed experimentally or explored for applications of spintronic THz emitters.

Introduction.—The femtosecond (fs) laser pulse (fsLP)-driven magnetic layer [1] is a far from equilibrium [2, 3] quantum many-body system with very different properties [4] when compared to the same material in equilibrium. It exhibits complex angular momentum exchange between photons, electrons and ionic cores [5, 6], rapidly emerging over ~ 10 fs time segments [7, 8]. They conspire to produce ultrafast *demagnetization* as experimentally observable phenomenon [1, 7, 8], where magnetization vector is decreasing its length along the easy (chosen as the z-) axis while *not* rotating

$$\frac{M_z(t)}{M_z(t=0)} < 1; M_x(t) = M_y(t) = 0. \tag{1}$$

That is, its x- and y-components remain zero or negligible [6, 9], as illustrated by experimental data [7] in Fig. 1 for single Ni ferromagnetic (FM) layer. Here $M_z(t=0)$ is the magnitude of magnetization in equilibrium, i.e., prior to fsLP application. Even a single FM layer exhibiting ultrafast demagnetization emits THz electromagnetic (EM) radiation [10], but such radiation in 0.1–30 THz frequency range relevant for applications [11] becomes greatly enhanced [12–14] when FM layer is brought into a contact with nonmagnetic (NM) layer hosting strong spin-orbit coupling (SOC) in the bulk or at the interface [15–17]. Experiments also observe [18] much faster demagnetization rate in FM/NM bilayers.

Although insights into microscopic mechanisms causing demagnetization have been greatly developed, primarily through first-principles studies based on time-dependent density functional theory (TDDFT) [5, 6] and its extensions [19], the origin of THz radiation remains a puzzle. For example, such radiation from a single FM layer has been explained as being magnetic dipole radiation by time-dependent magnetization [10], but recent detailed TDDFT+Maxwell calculations [9] show that such source is many orders of magnitude weaker than time-dependent charges (as it could be expected due to magnetic effects being, in general, $1/c$ smaller than electric ones). In the case of FM/NM bilayers, experiments standardly postulate [12–14, 20] the presence of spin current flowing from FM to NM layer, which is then converted into charge current within NM layer by the inverse spin Hall effect (ISHE) [21], or at FM/NM interface by other SOC driven mechanisms [15–17]. Such charge current within NM layer flows parallel to FM/NM interface, as well as parallel to the initial motion of electrons within FM layer which follows the direction of the electric field of (typically linearly polarized) of fsLP.

Thus, the critical problems persist: *Why FM or FM/NM systems emit EM radiation of frequency so much smaller than that of incoming light? What is the role of demagnetization in it?* For example, the incoming light initially drives valence [6] electrons to respond at its own frequency (typically, fs pulse has a central wavelength of $\simeq 800$ nm), which is expected to lead only to high harmonics (at integer multiples of frequency of incoming light) of emitted radiation as frequently observed in the

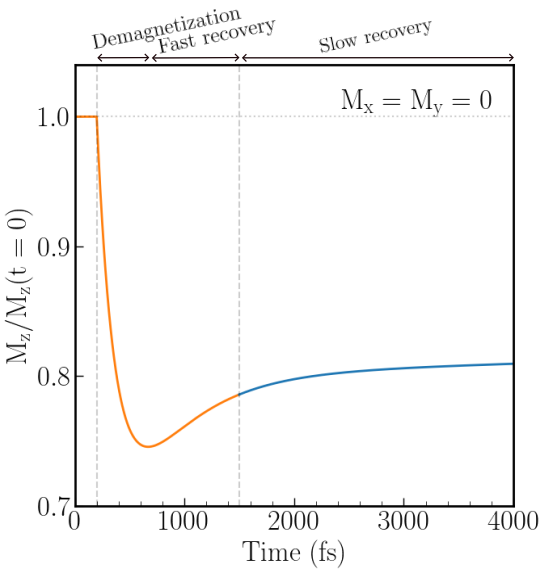

FIG. 1. Example of demagnetization dynamics [Eq. (1)] in ultrafast-light-driven single layer of Ni, as extracted by *probe* light of time- and angle-resolved photoelectron spectroscopy correlated with time-resolved transverse magneto-optical Kerr effect in Ref. [7] (reproduced from Fig. 1A in it). The *pump* light in Ref. [7] exciting demagnetization dynamics is fsLP of duration $\simeq 28$ fs and central wavelength 780 nm.

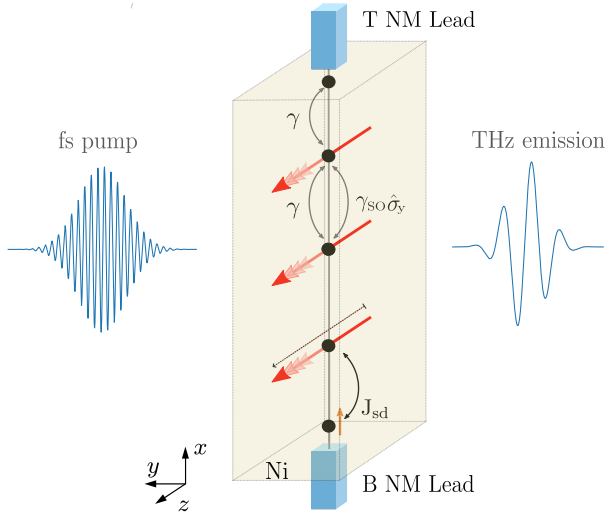

FIG. 2. Schematic view of a two-terminal setup—FM central region [modeled by 1D TB chain in Eq. (2)] connected to semi-infinite B and T NM leads—which is *standardly employed* in theoretical studies of spin [24, 25] and charge [26, 27] pumping by microwave-driven magnetization precessing with periodic time dependence. Instead of precessing magnetization, we use LMMs which only change length while not rotating [Eq. (1)], where such nonperiodic time-dependence of demagnetization is taken from experimental data in Fig. 1. The setup can also be viewed as 1D chain of atoms isolated from realistic [7] ultrafast-light-driven Ni layer. Time-dependent $m_i^z(t)$ leads to pumping of *both* charge and spin currents [Fig. 3], which we compute via TDNEGF algorithms [28–31] that can handle *arbitrary* time-dependence within the central region.

case of nonmagnetic materials [22] (high harmonics are also present [2] in the case of light-driven magnetic materials, but rarely explored experimentally). The usually invoked phenomenological picture of spin voltage (or accumulation) [14, 23], as a difference between nonequilibrium chemical potentials of the two spin species, which drives spin current from FM to NM layer does not explain its frequency spectrum containing features in the THz range or the role played by magnetization varying according to Eq. (1). For example, the very recent TDDFT study [9] shows that when electrons respond to light pulse, while magnetization is artificially frozen in time, no spin current flows from FM to NM layer even though spin voltage remains nonzero in such situation.

Thus, time-dependent magnetization [Eq. (1)] as the necessary ingredient to obtain spin current from FM to NM layer points at it being an additional mechanism driving quantum subsystem of electrons out of equilibrium, thereby generating charge currents. We recall that mechanisms of quantum charge and spin pumping [32] by time-dependent fields, and in the absence of any DC bias voltage (hence term "pumping"), have been amply explored in nanostructures driven by time-dependent gate voltages [33, 34], as well as in magnetic heterostructures [24, 25, 35] driven by microwave (or sub-THz in the case of antiferromagentic layers [36, 37]) radiation to cause their magnetization into steady precession. In all of these cases, the driving field has periodic time dependence and its frequency is sufficiently small to perturb the system only slightly out of equilibrium. For example, the energy of microwave photons $\hbar\omega \sim 10^{-6}$ eV is much smaller than the Fermi energy, $\hbar\omega \ll E_F$, so that FM layer with precessing magnetization, acting as periodic time-dependent field that pumps spin current, is in the linear-response regime [38]. These problems offer a blueprint of accomplished fully microscopic understanding, where one starts from time-dependent Hamiltonian (including possible first-principles ones [37, 39]) and obtains pumped spin and/or charge currents from rigorous quantum transport theory [26, 27, 34, 40].

The ultrafast-light-driven FM systems appear at first sight quite different from standard spin pumping [24, 25, 35] by precessing magnetization of fixed length—they are far from equilibrium (i.e., with dramatically modified electronic spectrum [2, 3]) and having nonprecessing [Eq. (1)], nonperiodic [Fig. 1] and shrinking in length magnetization. Nonetheless, in this Letter we *directly connect* these two disparate phenomena. For this purpose, we use the same setup employed in standard spin pumping theory [24–27, 37, 39] where FM central region is sandwiched between two semi-infinite NM leads [Fig. 2]. But we replace precessing localized magnetic moments (LMMs) $\mathbf{m}_i(t)$ at sites i of FM central region (where, e.g., m_i^z is constant and $m_i^x(t)$ and $m_i^y(t)$ change

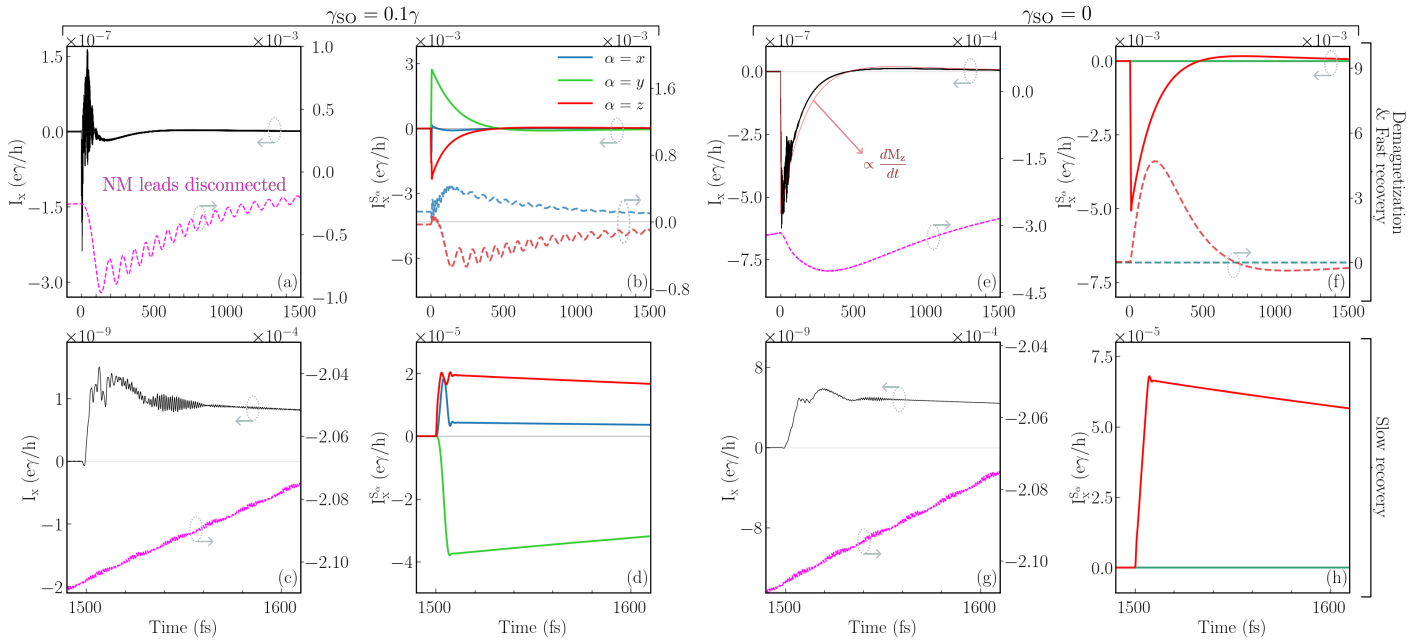

FIG. 3. Charge I_x and spin $I_x^{S_\alpha}$ currents along the x-axis pumped by demagnetization dynamics [Fig. 1] of fsLP-driven single Ni layer in: (a)–(d) the presence of SOC coupling [$\gamma_{SO} \neq 0$ in Eq. (2)]; or (e)–(h) the absence of SOC coupling [$\gamma_{SO} \neq 0$ in Eq. (2)]. Panel (e) also shows (thin red line) time derivative dM_z/dt. Panels (a),(b),(e) and (f) are obtained during demagnetization & fast recovery time interval from experimental data in Fig. 1, while panels (c),(d),(g) and (h) are obtained during slow recovery. I_x and $I_x^{S_\alpha}$ are computed either in the T NM lead in Fig. 2; or across the top edge bond ($19 \rightarrow 20$) of FM central region when NM leads are disconnected (dashed lines; for all solid lines, NM leads in Fig. 2 are connected).

harmonically in time, while $|\mathbf{m}_i(t)| = \text{const.}$ [25, 27]) with $m_i^z(t)$ decreasing according to demagnetization dynamics [Eq. (1)] of experimental data [7] in Fig. 1. Note that the sum of LMMs gives total magnetization, $\mathbf{M} = \sum_i \mathbf{m}_i$, where in the case of standard spin pumping computed via the scattering matrix-based Brouwer formula [34] one obtains [24, 25] for the vector of pumped spin current $(I^{S_x}_{\text{FM}\rightarrow\text{NM}}, I^{S_y}_{\text{FM}\rightarrow\text{NM}}, I^{S_z}_{\text{FM}\rightarrow\text{NM}}) \propto \mathbf{M} \times d\mathbf{M}/dt$. Naïve application of this expression to the setup in Fig. 2 would give zero pumped current as $\mathbf{M} \parallel d\mathbf{M}/dt$ [Eq. (1)] in the case of demagnetization. Nevertheless, since $\mathbf{M}(t)$ is not periodic in the course of demagnetization, neither scattering matrix-based Brouwer formula [34] nor more general Floquet-scattering-matrix formulas [27, 40] are applicable to two-terminal setup in Fig. 2. Instead, we employ time-dependent nonequilibrium Green's function (TDNEGF) algorithms [28, 29] which can handle arbitrary time dependence of the central region in the two-terminal setup of Fig. 2. For simplicity, the central FM region in Fig. 2 is modeled as a one-dimensional (1D) tight-binding (TB) chain, and NM leads are modeled as semi-infinite TB chains which terminate at infinity into macroscopic reservoirs of electrons kept at the same chemical potential. This setup can also be viewed [Fig. 2] as a chain of atoms we isolate from a realistic Ni layer, where incoming linearly polarized laser light with electric field oscillating along the chain (the x-axis) causes

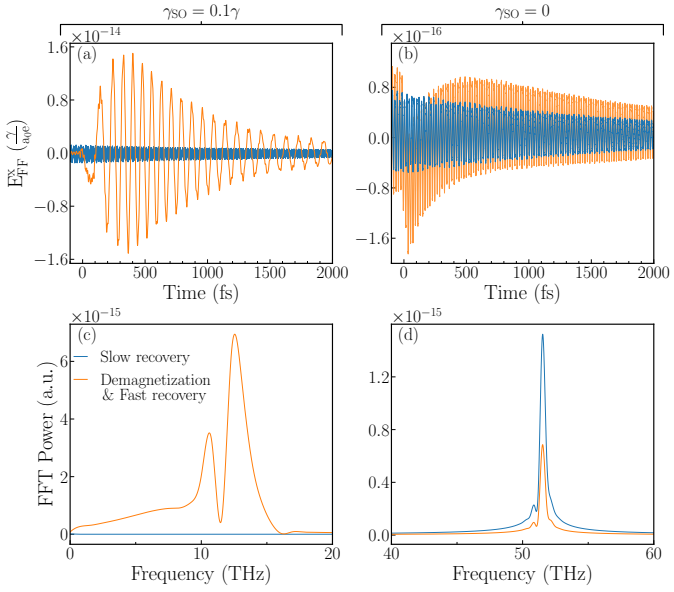

FIG. 4. (a) Time-dependence of the x-component of electric field E^x_{FF} of EM radiation in the far field region, as generated by pumped charge bond currents from Figs. 3(a) [orange line] and 3(c) [blue line] in the presence of SOC. (b) Same information as in (a), but using pumped charge bond currents from Figs. 3(e) and Figs. 3(g) in the absence of SOC. (c) and (d) FFT power of signals in panels (a) and (b), respectively.

demagnetization dynamics along the z-axis. Such geometry is often encountered experimentally (see, e.g., Fig. 1 in Ref. [20]) or in TDDFT calculations (see, e.g., Fig. 1 in Ref. [9]). Since experimental setups used in ultrafast demagnetization *do not* contain NM leads, reservoirs and external circuit attached—in contrast to standard pumping problems studied in nanoscale devices [32, 33] or magnetic multilayers [35]—we also analyze setup in Fig. 2 whose semi-infinite NM leads are disconnected (due to very small hopping toward them) and pumped currents (dashed lines in Fig. 3) are forced to reflect from the boundaries of the FM central region. Our principal results in Figs. 3 and 4 demonstrate what kind of currents are pumped by demagnetization dynamics and the frequency spectrum of EM radiation due to time-derivative of pumped charge current [Eq. (5)], respectively. We find that demagnetization dynamics pumps *both* charge and (one component of, $I_x^{S_z}$) spin currents, even in the absence of any SOC within FM central region [Fig. 3(e)–(g)]. This is quite *surprising* when compared to standard pumping by precessing magnetization where charge pumping is found only under special conditions, such as SOC present in the bulk [27] of FM layer, or at FM/NM interface [26], as confirmed experimentally [41]. With SOC absent and NM leads attached, we also find [Figs. 3(e),(f)] that during demagnetization pumped currents follow dM_z/dt. This provides some justification for "dM/dt mechanism" conjectured [14, 42, 43] from fitting of experimental data. However, with leads disconnected and/or in the presence of SOC—which is typically the case as SOC provides magnetic anisotropy in FM layers in equilibrium or plays an essential role [6, 8] out of equilibrium by triggering spin-flips [19] responsible for demagnetization—pumped currents proportionality to dM_z/dt is lost in Fig. 3. In addition, all three components of pumped spin current [Figs. 3(b),(d)] become nonzero in the presence of SOC.

Time-dependent charge currents [Figs. 3(a),(e)] will inevitably radiate EM waves, even if conversion of additionally pumped spin current [Figs. 3(b),(f)] into charge current is: absent, as in case of a single FM layer [10]; inefficient [44]; or not easily related [45] to the source of experimentally observed THz radiation. We use the Jefimenko equations [46, 47], as properly time-retarded solutions of the Maxwell equations in the case when time-dependent charges and their current can be considered as given [9], to compute electric field $\mathbf{E}_{\rm FF}$ [Eq. (5)] of emitted EM radiation in the so-called far field (FF) region (where electric field decays as inverse of distance from the source). The Jefimenko formula for $\mathbf{E}_{\rm FF}$ reveals that it is radiated only by the *time-derivative* of local [or bond, $I_{i\to j}$, in Eqs. (5) and (6)] charge currents, rather than by charge current itself as often assumed in fitting of experimental data [14, 20]. By plugging into Eq. (5) bond charge currents from realistic setup with disconnected NM leads, i.e., magenta curves from Figs. 3(a) and 3(e), we obtain $E_{\rm FF}^x$ in Figs. 4(a) and 4(b), respectively. Their fast Fourier transform (FFT) in Figs. 4(c) and 4(d), respectively, demonstrates that charge currents pumped directly (i.e., *without* any spin-to-charge conversion) by demagnetization dynamics contain [orange line in Fig. 4(c)] spectral features within 0.1–30 THz range in full accord with experiments [12–17, 20]. By comparing Figs. 4(c) and 4(d), we learn that THz spectral features are related to SOC-induced oscillations in magenta line in Fig. 3(a).

Models and Methods.—The Hamiltonian of two-terminal setup of Fig. 2 is that of 1D TB chain

$$\begin{aligned}\hat{H}(t) &= -\gamma\sum_{\langle ij\rangle}\hat{c}_i^\dagger\hat{c}_j - J_{sd}\sum_i \hat{c}_i^\dagger\hat{\boldsymbol{\sigma}}\cdot\mathbf{m}_i(t)\hat{c}_i \\ &\quad -i\gamma_{\rm SO}\sum_{\langle ij\rangle}\hat{c}_i^\dagger\hat{\sigma}_y\hat{c}_j. \end{aligned} \tag{2}$$

The TB chain hosts both conduction electrons and classical LMMs $\mathbf{m}_i(t)$ to model metallic FM central region. The bottom (B) and the top (T) NM leads are also semi-infinite 1D TB chains, described by the first term alone in Eq. (2). The Fermi energy of the macroscopic reservoirs into which NM leads terminate is set at $E_F = 0$. Here $\hat{c}_i^\dagger = (\hat{c}_{i\uparrow}^\dagger \;\; \hat{c}_{i\downarrow}^\dagger)$ is a row vector containing operators $\hat{c}_{i\sigma}^\dagger$ which create an electron with spin $\sigma =\uparrow,\downarrow$ at site i; $\hat{c}_i$ is a column vector containing the corresponding annihilation operators; γ is the hopping between the nearest-neighbor (NN) sites, also setting the unit of energy; $\gamma_{\rm SO}$ is an additional spin-dependent hopping [48] due to the Rashba SOC [49]; and the conduction electron spin, described by the vector of the Pauli matrices $\hat{\boldsymbol{\sigma}} = (\hat{\sigma}_x, \hat{\sigma}_y, \hat{\sigma}_z)$, interacts with $\mathbf{m}_i(t)$, which remain parallel at all times to the z-axis while only changing their length [Eq. (1)] according to experimental data in Fig. 1, via *sd* exchange interaction of strength $J_{sd} = 0.2\gamma$ [50].

The fundamental quantity of quantum statistical mechanics is the density matrix. The time-dependent one-particle nonequilibrium density matrix can be expressed [28], $\boldsymbol{\rho}^{\rm neq}(t) = \hbar\mathbf{G}^<(t,t)/i$, in terms of the lesser Green's function of TDNEGF formalism [28] defined by $G_{ii'}^{<,\sigma\sigma'}(t,t') = \frac{i}{\hbar}\langle\hat{c}_{i'\sigma'}^\dagger(t')\hat{c}_{i\sigma}(t)\rangle_{\rm nes}$ where $\langle\ldots\rangle_{\rm nes}$ is the nonequilibrium statistical average [51]. We solve a matrix integro-differential equation [29, 30]

$$i\hbar\partial_t\boldsymbol{\rho}^{\rm neq} = [\mathbf{H}(t), \boldsymbol{\rho}^{\rm neq}] + i\sum_{p=B,T}[\boldsymbol{\Pi}_p(t) + \boldsymbol{\Pi}_p^\dagger(t)], \tag{3}$$

for the time evolution of $\boldsymbol{\rho}^{\rm neq}(t)$, where $\mathbf{H}(t)$ is the matrix representation of Hamiltonian in Eq. (2). Equation (3) is an *exact* quantum master equation for the reduced density matrix of the FM central region viewed as an open finite-size quantum system attached to macroscopic Fermi liquid reservoirs via semi-infinite NM leads. The $\boldsymbol{\Pi}_p(t)$ matrices

$$\boldsymbol{\Pi}_p(t) = \int_0^t dt_2\,[\mathbf{G}^>(t,t_2)\boldsymbol{\Sigma}_p^<(t_2,t) - \mathbf{G}^<(t,t_2)\boldsymbol{\Sigma}_p^>(t_2,t)], \tag{4}$$

are expressed in terms of the lesser and greater Green's functions [51] and the corresponding self-energies $\mathbf{\Sigma}_p^{>,<}(t,t')$ [29]. They yield directly time-dependent charge, $I_p(t) = \frac{e}{\hbar}\mathrm{Tr}\left[\mathbf{\Pi}_p(t)\right]$, and and spin current, $I_p^{S_\alpha}(t) = \frac{e}{\hbar}\mathrm{Tr}\left[\hat{\sigma}_\alpha\mathbf{\Pi}_p(t)\right]$, flowing into lead $p = B, T$ for *arbitrary* time-dependence of Hamiltonian of the central region. Since the applied bias voltage between NM leads is identically zero in this study, all computed $I_p(t)$ and $I_p^{S_\alpha}(t)$ are solely currents pumped by time-dependence of the Hamiltonian. We use the same units for charge and spin currents, defined as $I_p = I_p^\uparrow + I_p^\downarrow$ and $I_p^{S_\alpha} = I_p^\uparrow - I_p^\downarrow$, in terms of spin-resolved charge currents I_p^σ. In our convention, positive current in NM lead p means charge or spin current is flowing out of that lead.

The electric field of EM radiation emitted into the FF region is calculated from the Jefimenko equations [46], reorganized [47] to isolate FF contributions

$$\mathbf{E}_{\mathrm{FF}}(\mathbf{r},t) = \frac{1}{4\pi\epsilon_0 c^2}\sum_{P_{i\to j}=1}^{N_b}\int_{P_{i\to j}}\left[(\mathbf{r}-\mathbf{l})\frac{\partial_t I_{i\to j}(t_r)}{|\mathbf{r}-\mathbf{l}|^3}(\mathbf{r}-\mathbf{l})\cdot\mathbf{e}_x - \frac{\partial_t I_{i\to j}(t_r)}{|\mathbf{r}-\mathbf{l}|}\mathbf{e}_x\right]dl. \tag{5}$$

and adapted [2, 52] to take time-dependent bond charge currents, $I_{i\to j}(t)$ [Eq. (6)] defined on TB lattice, as the source. Here $t_r \equiv t - |\mathbf{r}-\mathbf{l}|/c$ emphasizes retardation in the response time due to relativistic causality [46, 47]. In Figs. 3 and 4, as well as in Eq. (5), we use $N = 20$ as the number of TB sites and $N_b = 19$ as the number of bonds between. The bond currents [30, 48, 52] $I_{i\to j}$ are assumed to be spatially homogeneous along the path $P_{i\to j}$ from site i to site j, which is composed of a set of points $l \in P_{i\to j}$. We obtain them as

$$I_{i\to j}(t) = \frac{e\gamma}{i\hbar}\mathrm{Tr}_{\mathrm{spin}}\left[\boldsymbol{\rho}_{ij}(t)\mathbf{H}_{ji}(t) - \boldsymbol{\rho}_{ji}(t)\mathbf{H}_{ij}(t)\right], \tag{6}$$

by isolating 2×2 submatrices $\boldsymbol{\rho}_{ij}^{\mathrm{neq}}(t)$ of $\boldsymbol{\rho}^{\mathrm{neq}}(t)$ whose off-diagonal elements determine such currents. Note that diagonal elements of $\boldsymbol{\rho}_{ij}^{\mathrm{neq}}(t)$ determine on-site nonequilibrium charge density, whose time dependence contributes [2, 9, 52] to near-field EM radiation. In Eq. (6) $\mathrm{Tr}_{\mathrm{spin}}[\ldots]$ denotes trace in the spin space only.

Conclusions and Outlook.—By using time dependence [Fig. 1] of ultrafast demagnetization [Eq. (1)] from experiments [7] on fsLP-driven Ni layer—which is plugged into a two-terminal setup [Fig. 2] of standard theory [24, 25] of spin pumping to replace its slowly and harmonically precessing magnetization of fixed length driven by microwave absorption [35]—we *directly connect* these two apparently disparate phenomena. That is, time-dependent quantum transport theory that can handle [28–31] arbitrary time-dependence of LMMs within the central FM region in Fig. 2 shows how demagnetization pumps, surprisingly, both spin and charge currents. The physical picture emerging is that of fsLP which drives electrons far from equilibrium to cause their current oscillating at light frequency (as well as at high harmonics of light frequency [2, 22]), while the ensuing [6] demagnetization dynamics pumps additional charge current whose time derivative [Eq. (5)] generates spectral features of emitted EM radiation at THz frequencies in Fig. 4(c) [additional Fig. S1 in the Supplemental Material [53] demonstrates that presence of *both* fsLP and demagnetization dynamics as concurrent nonequilibirum drives does not change our conclusions from Fig. 4(c)]. We emphasize that slow recovery [Fig. 1] of magnetization on longer ~ 1 ps timescales *does not* generate any EM radiation with features in 0.1–30 THz range [Fig. 4(d)]. Our prediction of direct charge pumping by ultrafast demagnetization dynamics offers a unified explanation for experimentally observed THz radiation from both single FM layer [10] and FM/NM bilayers [12–14, 20]. It can be easily *confirmed or falsified* by observing THz radiation from, e.g., Pt/Ni/Pt trilayer whose intensity is comparable to the one from often employed [20] Ni/Pt bilayer. In contrast, standard phenomenological picture [12–14, 20] of spin-to-charge current conversion by ISHE in Pt would *predict no* EM radiation from Pt/Ni/Pt trilayer due to opposite direction of ISHE charge currents within two Pt layers. Even if much smaller THz radiation is found in Pt/Ni/Pt trilayer, our theory still provides microscopic explanation for the origin of spin current flowing from Ni to Pt layer, thereby replacing phenomenologically conjectured spin voltage [14, 23] as its driving mechanism.

This research was primarily supported by NSF through the University of Delaware Materials Research Science and Engineering Center, DMR-2011824. The supercomputing time was provided by DARWIN (Delaware Advanced Research Workforce and Innovation Network), which is supported by NSF Grant No. MRI-1919839.

* bnikolic@udel.edu

[1] E. Beaurepaire, J.-C. Merle, A. Daunois, and J.-Y. Bigot, Ultrafast spin dynamics in ferromagnetic nickel, Phys. Rev. Lett. **76**, 4250 (1996).

[2] A. Suresh and B. K. Nikolić, Quantum classical approach to spin and charge pumping and the ensuing radiation in terahertz spintronics: Example of the ultrafast light-

driven Weyl antiferromagnet Mn_3Sn, Phys. Rev. B **107**, 174421 (2023).
[3] K. Gillmeister, D. Golež, C.-T. Chiang, N. Bittner, Y. Pavlyukh, J. Berakdar, P. Werner, and W. Widdra, Ultrafast coupled charge and spin dynamics in strongly correlated NiO, Nat. Commun. **11**, 4095 (2020).
[4] A. V. Kimel and M. Li, Writing magnetic memory with ultrashort light pulses, Nat. Rev. Mater. **4**, 189 (2019).
[5] Z. Chen and L.-W. Wang, Role of initial magnetic disorder: A time-dependent ab initio study of ultrafast demagnetization mechanisms, Sci. Adv. **5**, eaau800 (2019).
[6] K. Krieger, J. K. Dewhurst, P. Elliott, S. Sharma, and E. K. U. Gross, Laser-induced demagnetization at ultrashort time scales: Predictions of TDDFT, J. Chem. Theory Comput. **11**, 4870 (2015).
[7] P. Tengdin, W. You, C. Chen, X. Shi, D. Zusin, Y. Zhang, C. Gentry, A. Blonsky, M. Keller, P. M. Oppeneer, *et al.*, Critical behavior within 20 fs drives the out-of-equilibrium laser-induced magnetic phase transition in nickel, Sci. Adv. **4**, eaap974 (2018).
[8] F. Siegrist, J. A. Gessner, M. Ossiander, C. Denker, Y.-P. Chang, M. C. Schröder, A. Guggenmos, Y. Cui, J. Walowski, U. Martens, *et al.*, Light-wave dynamic control of magnetism, Nature **571**, 240 (2019).
[9] A. Kefayati and B. K. Nikolić, Electromagnetic radiation from ultrafast-light-driven spintronic thz emitters: A time-dependent density functional theory plus Jefimenko equations approach, arXiv:2312.04476 (2023).
[10] E. Beaurepaire, G. M. Turner, S. M. Harrel, M. C. Beard, J.-Y. Bigot, and C. A. Schmuttenmaer, Coherent terahertz emission from ferromagnetic films excited by femtosecond laser pulses, Appl. Phys. Lett. **84**, 3465 (2004).
[11] A. Leitenstorfer, A. S. Moskalenko, T. Kampfrath, J. Kono, E. Castro-Camus, K. Peng, N. Qureshi, D. Turchinovich, K. Tanaka, A. G. Markelz, *et al.*, The 2023 terahertz science and technology roadmap, J. Phys. D **56**, 223001 (2023).
[12] T. Seifert, S. Jaiswal, U. Martens, J. Hannegan, L. Braun, P. Maldonado, F. Freimuth, A. Kronenberg, J. Henrizi, I. Radu, *et al.*, Efficient metallic spintronic emitters of ultrabroadband terahertz radiation, Nat. Photonics **10**, 483 (2016).
[13] Y. Wu, M. Elyasi, X. Qiu, M. Chen, Y. Liu, L. Ke, and H. Yang, High-performance THz emitters based on ferromagnetic/nonmagnetic heterostructures, Adv. Mater. **29**, 1603031 (2017).
[14] R. Rouzegar, L. Brandt, L. c. v. Nádvorník, D. A. Reiss, A. L. Chekhov, O. Gueckstock, C. In, M. Wolf, T. S. Seifert, W. Brouwer, *et al.*, Laser-induced terahertz spin transport in magnetic nanostructures arises from the same force as ultrafast demagnetization, Phys. Rev. B **106**, 144427 (2022).
[15] M. B. Jungfleisch, Q. Zhang, W. Zhang, J. E. Pearson, R. D. Schaller, H. Wen, and A. Hoffmann, Control of terahertz emission by ultrafast spin-charge current conversion at Rashba interfaces, Phys. Rev. Lett. **120**, 207207 (2018).
[16] O. Gueckstock, L. Nádvorník, M. Gradhand, T. S. Seifert, G. Bierhance, R. Rouzegar, M. Wolf, M. Vafaee, J. Cramer, M. A. Syskaki, *et al.*, Terahertz spin-to-charge conversion by interfacial skew scattering in metallic bilayers, Adv. Mater. **33**, 2006281 (2021).
[17] Y. Wang, W. Li, H. Cheng, Z. Liu, Z. Cui, J. Huang, B. Xiong, J. Yang, H. Huang, J. Wang, *et al.*, Enhancement of spintronic terahertz emission enabled by increasing Hall angle and interfacial skew scattering, Commun. Phys. **6**, 280 (2023).
[18] K. C. Kuiper, T. Roth, A. J. Schellekens, O. Schmitt, B. Koopmans, M. Cinchetti, and M. Aeschlimann, Spin-orbit enhanced demagnetization rate in Co/Pt-multilayers, Appl. Phys. Lett. **105**, 202402 (2014).
[19] S. R. Acharya, V. Turkowski, G. P. Zhang, and T. S. Rahman, Ultrafast electron correlations and memory effects at work: Femtosecond demagnetization in Ni, Phys. Rev. Lett. **125**, 017202 (2020).
[20] T. S. Seifert, D. Go, H. Hayashi, R. Rouzegar, F. Freimuth, K. Ando, Y. Mokrousov, and T. Kampfrath, Time-domain observation of ballistic orbital-angular-momentum currents with giant relaxation length in tungsten, Nat. Nanotechnol. **18**, 1132 (2023).
[21] E. Saitoh, M. Ueda, H. Miyajima, and G. Tatara, Conversion of spin current into charge current at room temperature: Inverse spin-Hall effect, Appl. Phys. Lett. **88**, 182509 (2006).
[22] S. Ghimire and D. A. Reis, High-harmonic generation from solids, Nat. Phys. **15**, 10 (2018).
[23] K. Bühlmann, G. Saerens, A. Vaterlaus, and Y. Acremann, Detection of femtosecond spin voltage pulses in a thin iron film, Struct. Dyn. **7**, 065101 (2020).
[24] Y. Tserkovnyak, A. Brataas, and G. E. W. Bauer, Enhanced Gilbert damping in thin ferromagnetic films, Phys. Rev. Lett. **88**, 117601 (2002).
[25] Y. Tserkovnyak, A. Brataas, G. E. Bauer, and B. I. Halperin, Nonlocal magnetization dynamics in ferromagnetic heterostructures, Rev. Mod. Phys. **77**, 1375 (2005).
[26] F. Mahfouzi, J. Fabian, N. Nagaosa, and B. K. Nikolić, Charge pumping by magnetization dynamics in magnetic and semimagnetic tunnel junctions with interfacial Rashba or bulk extrinsic spin-orbit coupling, Phys. Rev. B **85**, 054406 (2012).
[27] J. Varela-Manjarres and B. K. Nikolić, High-harmonic generation in spin and charge current pumping at ferromagnetic or antiferromagnetic resonance in the presence of spin-orbit coupling, J. Phys. Mater. **6**, 045001 (2023).
[28] B. Gaury, J. Weston, M. Santin, M. Houzet, C. Groth, and X. Waintal, Numerical simulations of time-resolved quantum electronics, Phys. Rep. **534**, 1 (2014).
[29] B. S. Popescu and A. Croy, Efficient auxiliary-mode approach for time-dependent nanoelectronics, New J. Phys. **18**, 093044 (2016).
[30] M. D. Petrović, B. S. Popescu, U. Bajpai, P. Plecháč, and B. K. Nikolić, Spin and charge pumping by a steady or pulse-current-driven magnetic domain wall: A self-consistent multiscale time-dependent quantum-classical hybrid approach, Phys. Rev. Appl. **10**, 054038 (2018).
[31] M. D. Petrović, U. Bajpai, P. Plecháč, and B. K. Nikolić, Annihilation of topological solitons in magnetism with spin-wave burst finale: Role of nonequilibrium electrons causing nonlocal damping and spin pumping over ultrabroadband frequency range, Phys. Rev. B **104**, L020407 (2021).
[32] R. Citro and M. Aidelsburger, Thouless pumping and topology, Nat. Rev. Phys. **5**, 87 (2023).
[33] M. Switkes, C. M. Marcus, K. Campman, and A. C. Gossard, An adiabatic quantum electron pump, Science **283**, 1905 (1999).
[34] P. W. Brouwer, Scattering approach to parametric pumping, Phys. Rev. B **58**, R10135 (1998).

[35] K. Ando, Dynamical generation of spin currents, Semicond. Sci. Technol. **29**, 043002 (2014).

[36] P. Vaidya, S. A. Morley, J. van Tol, Y. Liu, R. Cheng, A. Brataas, D. Lederman, and E. del Barco, Subterahertz spin pumping from an insulating antiferromagnet, Science **368**, 160 (2020).

[37] K. Dolui, A. Suresh, and B. K. Nikolić, Spin pumping from antiferromagnetic insulator spin-orbit-proximitized by adjacent heavy metal: a first-principles Floquet-nonequilibrium Green function study, J. Phys. Mater. **5**, 034002 (2022).

[38] S.-H. Chen, C.-R. Chang, J. Q. Xiao, and B. K. Nikolić, Spin and charge pumping in magnetic tunnel junctions with precessing magnetization: A nonequilibrium Green function approach, Phys. Rev. B **79**, 054424 (2009).

[39] K. Dolui, U. Bajpai, and B. K. Nikolić, Effective spin-mixing conductance of topological-insulator/ferromagnet and heavy-metal/ferromagnet spin-orbit-coupled interfaces: A first-principles Floquet-nonequilibrium Green function approach, Phys. Rev. Mater. **4**, 121201 (2020).

[40] M. Moskalets, *Scattering Matrix Approach to Non-Stationary Quantum Transport* (Imeprial College Press, London, 2011).

[41] C. Ciccarelli, K. M. D. Hals, A. Irvine, V. Novak, Y. Tserkovnyak, H. Kurebayashi, A. Brataas, and A. Ferguson, Magnonic charge pumping via spin–orbit coupling, Nat. Nanotechnol. **10**, 50 (2015).

[42] G.-M. Choi, B.-C. Min, K.-J. Lee, and D. G. Cahill, Spin current generated by thermally driven ultrafast demagnetization, Nat. Commun. **5**, 4334 (2014).

[43] T. Lichtenberg, M. Beens, M. H. Jansen, B. Koopmans, and R. A. Duine, Probing optically induced spin currents using terahertz spin waves in noncollinear magnetic bilayers, Phys. Rev. B **105**, 144416 (2022).

[44] J. Gorchon, S. Mangin, M. Hehn, and G. Malinowski, Is terahertz emission a good probe of the spin current attenuation length?, Appl. Phys. Lett. **121**, 012402 (2022).

[45] G. Schmidt, B. Das-Mohapatra, and E. T. Papaioannou, Charge dynamics in spintronic terahertz emitters, Phys. Rev. Appl. **19**, L041001 (2023).

[46] O. D. Jefimenko, *Electricity and Magnetism* (Appleton Century-Crofts, New York, 1966).

[47] K. T. McDonald, The relation between expressions for time-dependent electromagnetic fields given by Jefimenko and by Panofsky and Phillips, Am. J. Phys. **65**, 1074 (1997).

[48] B. K. Nikolić, L. P. Zârbo, and S. Souma, Imaging mesoscopic spin Hall flow: Spatial distribution of local spin currents and spin densities in and out of multiterminal spin-orbit coupled semiconductor nanostructures, Phys. Rev. B **73**, 075303 (2006).

[49] A. Manchon, H. C. Koo, J. Nitta, S. M. Frolov, and R. A. Duine, New perspectives for Rashba spin–orbit coupling, Nat. Mater. **14**, 871 (2015).

[50] R. L. Cooper and E. A. Uehling, Ferromagnetic resonance and spin diffusion in supermalloy, Phys. Rev. **164**, 662 (1967).

[51] G. Stefanucci and R. Van Leeuwen, *Nonequilibrium many-body theory of quantum systems: a modern introduction* (Cambridge University Press, 2013).

[52] M. Ridley, L. Kantorovich, R. van Leeuwen, and R. Tuovinen, Quantum interference and the time-dependent radiation of nanojunctions, Phys. Rev. B **103**, 115439 (2021).

[53] See Supplemental Material at `https://wiki.physics.udel.edu/qttg/Publications`, which includes Ref. [54], for additional Fig. S1 which plots orange curves from Figs. 4(a) and 4(c), obtained when only demagnetization dynamics drives electrons out of equilibrium, as well as their two counterpart where both fsLP and demagnetization dynamics or just fsLP are present as generators of electronic currents.

[54] U. Bajpai, B. S. Popescu, P. Plecháč, B. K. Nikolić, L. E. F. F. Torres, H. Ishizuka, and N. Nagaosa, Spatiotemporal dynamics of shift current quantum pumping by femtosecond light pulse, J. Phys.: Mater. **2**, 025004 (2019).

Supplemental Material for "Charge and spin current pumping by ultrafast demagnetization dynamics"

Jalil Varela-Manjarres, Ali Kefayati, M. Benjamin Jungfleisch, John Q. Xiao, and Branislav K. Nikolić*
Department of Physics and Astronomy, University of Delaware, Newark, DE 19716, USA

This Supplemental Material provides one additional Fig. S1 demonstrating that main conclusion from Figs. 4(a) and 4(c) in the main text—that demagnetization dynamics is crucial to generate charge current with proper spectral features in 0.1–30 THz range—remain intact even if second nonequilibrium drive, that is fs laser pulse, is explicitly included. For this purpose, we copy orange curves from Figs. 4(a) and 4(c) into Fig. S1(a) and S1(b), respectively, and compare them with additional curves obtained when both fs laser pulse and demagnetization are operative, or only fs laser pulse is present. In particular, light alone cannot generate THz features of emitted electromagnetic radiation as its frequency is much higher, and any electronic current photoexcited by light directly will have spectral features either at that frequency or its high harmonics [1].

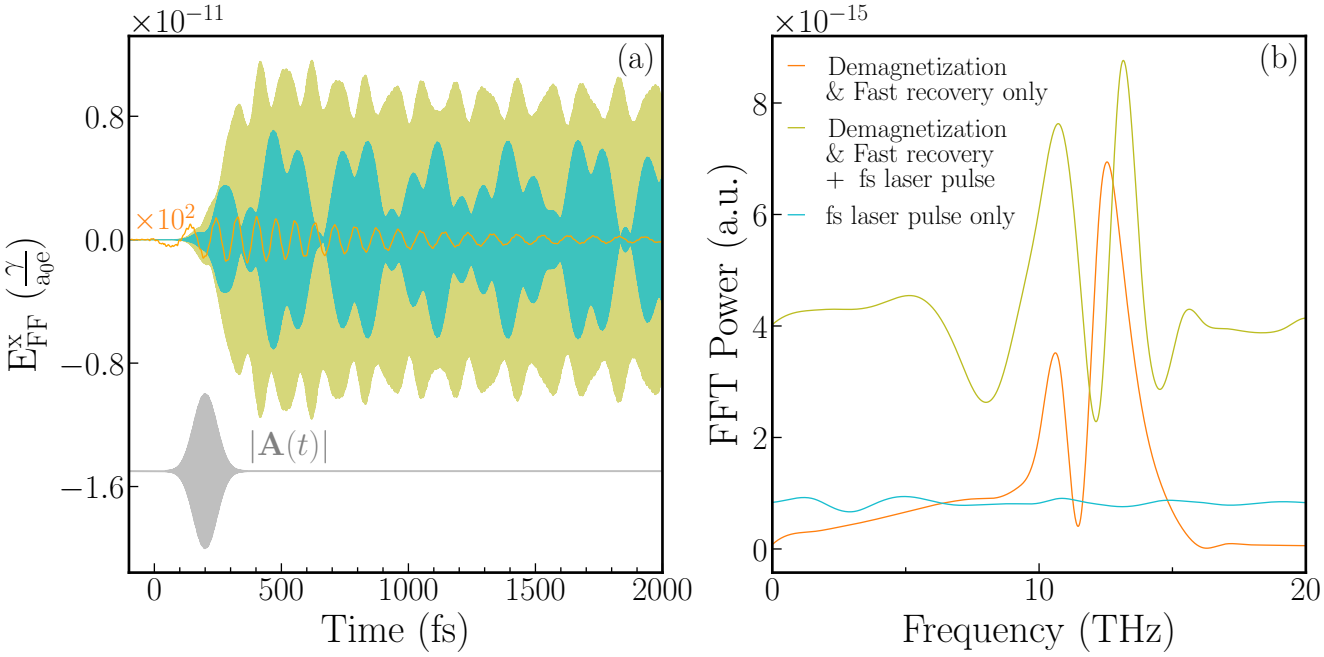

FIG. S1. (a) Time-dependence of the x-component of the electric field $E^x_{\rm FF}$ of electromagnetic (EM) radiation in the far-field region. Three signals in (a) are computed by plugging it charge currents into Jefimenko Eq. (5) in the main text obtained for: demagnetization & fast recovery dynamics (from Fig. 1 in the main text only) present as nonequilibrium drive [orange curve, which is identical to orange curve in Fig. 4(a) in the main text]; fs laser pulse only is present; and both of these nonequilibrium drives are present. (b) The corresponding fast Fourier transform (FFT) of three signals from panel (a). The fs light pulse driving electrons out of equilibrium is introduced via the Peierls substitution, as in Ref. [2] while using parameters $z_{\rm max} = 0.25$, $\sigma_{\rm light} = 2 \times 10^3$, $t_p = 200$ fs and central frequency $\hbar\omega_0 = 2.28$ eV. The gray curve on the bottom of panel (a) illustrates vector potential and duration of fs light pulse.

[1] A. Suresh and B. K. Nikolić, Quantum classical approach to spin and charge pumping and the ensuing radiation in terahertz spintronics: Example of the ultrafast light-driven Weyl antiferromagnet Mn_3Sn, Phys. Rev. B **107**, 174421 (2023).
[2] U. Bajpai, B. S. Popescu, P. Plecháč, B. K. Nikolić, L. E. F. F. Torres, H. Ishizuka, and N. Nagaosa, Spatio-temporal dynamics of shift current quantum pumping by femtosecond light pulse, J. Phys.: Mater. **2**, 025004 (2019).

* bnikolic@udel.edu